2018

CFD Simulation Of A Two Stage Twin Screw Compressor Including Leakage Flows And Comparison With Experimental Data

Rainer Andres
CFX Berlin Software GmbH, Germany, rainer.andres@cfx-berlin.de

Jan Hesse
CFX Berlin Software GmbH, Germany, jan.hesse@cfx-berlin.de

Farai Hetze
CFX Berlin Software GmbH, Germany, farai.hetze@cfx-berlin.de

Donald Low
Sullair A Hitachi Group Company, United States, donald.low@sullair.com

CFD SIMULATION OF A TWO STAGE TWIN SCREW COMPRESSOR INCLUDING LEAKAGE FLOWS AND COMPARISON WITH EXPERIMENTAL DATA

Rainer ANDRES[1]*, Jan HESSE[1], Farai HETZE[1], Donald LOW[2]

[1]CFX Berlin Software GmbH,
Berlin, Germany
rainer.andres@cfx-berlin.de

[2]Sullair
A Hitachi Group Company
Michigan City, United States
donald.low@sullair.com

* Corresponding Author

ABSTRACT

Computational Fluid Dynamics (CFD) is a common and validated simulation method in research and industry for the analysis of fluid systems. In the past years, it has proven to become more and more applicable for modeling the flow physics inside positive displacement (PD) machines. The working chamber and thus the discretized flow domain of PD machines are changing in time, characterized by complex thermodynamics. Compressible fluids, real-gas properties and leakage flows with trans- or supersonic characteristics are phenomena which have to be accounted for in order to properly model the behavior of the machine. As CFD methods evolve in general, but also for the application of PD machines in particular, the numerical model can replace a prototype during early stages of the product development. The desired simulation approach should be able to deliver sufficient accuracy at a feasible effort in terms of computational time and manpower to create the numerical model.

This paper presents the methodology of creating the numerical model for a sample screw compressor provided by Sullair for research purposes. It is a dry running two stage twin screw compressor running with air at a rated power range between 160 and 250 kW. The two stages are gear driven by the main shaft at rotational speeds between 1180 and 2100 rev/min. Each stage features different rotor profiles, where the first stage has a 4-6, the second stage a 5-7 lobe combination. The total pressure ratio of the two stages combined is up to 10:1. To enhance the performance of the compressor, discharged air from the first stage is cooled down before entering the second stage.

A specific meshing method is used to model the size-changing working chambers between rotors and casing, where only hexahedral cells are used and mesh topology is constant. The model accounts for radial and axial clearances between rotors and stator, where rotors and stator are connected with interfaces. The transient simulation results are compared to experimental measurements for torque, flow rate and volumetric efficiency. Also discharge pressure and temperature after first and second stage are compared to the experimental results. In addition, the possibilities of the simulation are exemplified by the gathering of time- and space-resolved monitor points like temperature or pressure at distinct points within the compressor.

Apart from direct comparison to the experiment, also a sensitivity study regarding the change of housing clearances is presented, as leakage flow has severe impact on the compressor performance. These clearances and the resulting leakages are often not exactly known whereas they also vary because of manufacturing tolerances or deformations due to the load on rotors and stator. Here, the numerical simulation can serve as a helpful tool to estimate the sensitivity and change of machine characteristics, which is hard to determine in the scope of experiments.

1. INTRODUCTION

While screw compressors are widely used in the industry, e. g. for pneumatic power tools or in the automotive industry oil free compressors are often used when purity of the air is critical. Within oil injected compressors, there is the risk of contaminated air which has an adverse effect on downstream processes and production. However, oil free compressors lack the sealing and cooling effect of the oil, thus in general the achieved pressure ratios are lower compared to oil flooded compressors. Compression ratio as well as the compression efficiency can be increased by using multi-stage compressors. The sample dry screw compressor from Sullair consists of two stages with pressure ratios up to 10:1 where each stage consists of two coaxial rotors. Furthermore, an intermediate cooler is located between the stages to cool the heated air discharged by the first stage in order to increase the compressor efficiency. For the manufacturer, reliable tools to evaluate overall machine performance such as compression ratio and power consumption as well as calculate losses and efficiency are of great desire. Also, the impact of design changes should be evaluated before actual prototypes are built so that developing costs can be reduced.

Screw compressors and their numerical simulation are quite complex, where for a multi-stage compressor, additional challenges are imposed. One approach is to treat both stages separately. However, this approach cannot describe direct interaction between the stages (e.g. pressure pulsation). Moreover, the requirement of setting a boundary condition at the discharge side of the first stage is apparent, since influence of the further downstream located second stage (and additional parts like an intermediate cooler) is a priori not known. Thus, an iterative simulation loop can be necessary in order to get a consistent solution.

The paper presents another strategy, where both compressor stages are coupled by including them in a single simulation run. The modeling methodology is analogue to single stage screw compressors. The deforming rotor chambers are separated and meshed independently from the stator parts and connected for the simulation run via fluid-fluid interfaces. During the transient run, rotor chamber meshes are deformed according to the current rotor position. For the modeled two stage screw compressor in this paper, both stages feature different rotor profiles with different rotating speeds, which the rotor chamber modeling has to account for. Also the intermediate cooler is modeled in a simplified way in the simulation setup, by decreasing the temperature between the two stages. The paper presents the modeling approach for a simplified setup (e. g. simplified cooler, adiabatic walls) to evaluate the feasibility of the CFD approach. For this purpose, achieved results are compared with measurements of the real compressor.

2. ROTOR CHAMBER MODELING

The spatial discretization of the rotor chambers can be realized with different approaches which all have to account for the deformation of the rotor chambers over time. The immersed solid method, remeshing or customized grid generation should be mentioned, where Spille-Kohoff (2015) points out the methodologies, advantages and disadvantages of the individual approaches more in detail. The numerical grids for the present screw compressor analysis are generated with the mesh generator TwinMesh, which provides automatically generated hexahedral grids for PD machines with two coaxial rotors. For the performed simulations, 3D meshes of the chamber volumes for all rotor positions that are considered in the transient simulation are generated prior to simulation. An O-type grid topology is used, where inflation layers in radial and axial direction are present to account for boundary layer resolution as well as a smooth volume change of grid cells towards axial clearances between rotors and housing. There are two O-type grids for each stage, which have a 1:1 connection. A detailed explanation of the utilized approach is given by Hesse (2014). A three dimensional view of the rotor chamber grids is shown in Figure 1.

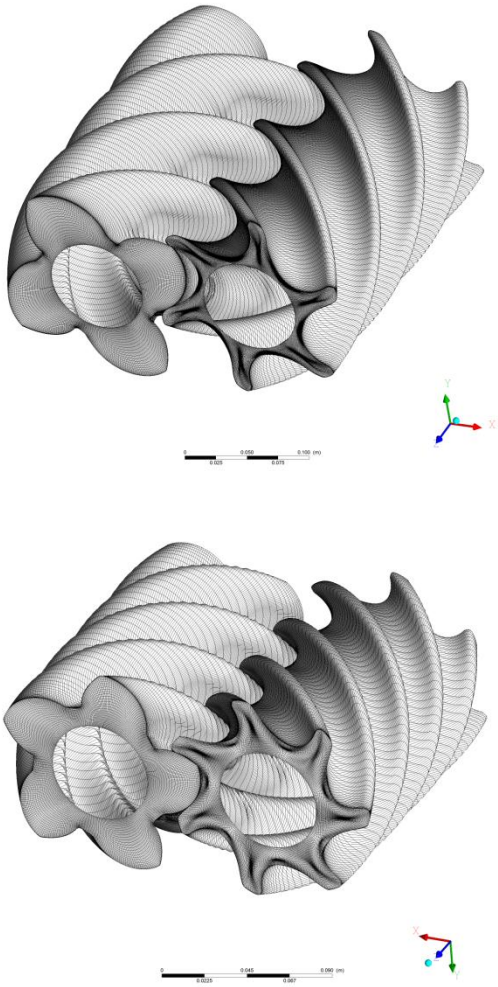

Figure 1: Grids for first stage (top) and second stage (bottom) of the compressor

Given that approach, it has to be considered that both compressor stages are modeled in one simulation setup, where the physical time step in the transient simulation is equal for the whole model. Thus, angle increments of the generated grids cannot be chosen arbitrarily for each stage. The ratio of angle increments for both stages has to represent the speed ratio of the two male rotors. The pitch angles and increments for both stages are given in the following table:

	Stage 1	Stage 2
Speed ratio (Stage 2/Stage 1)	1.53	
Pitch angle	90°	72°
Number of grids per pitch angle	90	47
Angle increment	1°	1.532°
Angle increment ratio (Stage2/Stage1)	1.532	

Table 1: Angle increments according to the speed ratio of the modeled two stage screw compressor

The angle increments are determined by a specified number of meshes per pitch angle, therefore the corresponding ratio slightly deviates from the exact ratio of 1.53. Hence the simulated revolution speed of the second stage will deviate from the reference value to the same small extend.

For both stages, rotational periodicity is taken into account in a way, that only the pitch angle for each stage (360° divided by the number of lobes of the male rotor) is meshed with a fixed angle increment. The resulting set of grids

enables to run the simulation for as many revolutions as required in order to get a periodic solution over time (i. e. the time averaged value of monitored flow quantities is constant over time). It should be noted, that reuse of the same grid sets for all subsequent rotation angles higher than the meshed pitch angle range is not generally possible. It requires that grid nodes (with fixed indices) are at the same location within the fluid volume for initial and last rotor position within the pitch angle range. If this is not the case, the simulation has to be restarted, where flow quantities from the final rotor chamber grid are interpolated to the first grid. For the presented simulation, grid nodes attached to the stator curves (i. e. the stator walls around the rotors) are fixed in space, while all others can move according to the rotor motion. In that way, it is ensured that node positions of first and last generated grid match and no interpolation is required to reuse the same grid set during the simulation run.

3. SIMULATION SETUP

All simulations for the sample Sullair screw compressor are performed in the commercial solver ANSYS CFX. Both stages are modeled within one case setup. The stator grids are connected to the rotor chamber grids with fluid-fluid interfaces, where the latter include the volume for the axial and radial clearances. During the simulation, the rotor positions and so the corresponding rotor chamber grids are updated automatically by a FORTRAN routine based on the generated grids prior to the simulation start.

The geometry of the intermediate cooler between the first and second stage is not discretized. Instead, the stages are connected with a free form duct, where the temperature loss caused by the cooler is modeled with an energy sink acting in the fluid volume of the duct. The location of the two stages relative to each other corresponds to the real compressor. Figure 2 shows the assembly of the case setup. The pressure loss due to the cooler was not measured in the experiment. It is expected to be in the magnitude of 0.10 to 0.15 bar. In the present setup, no pressure loss is defined in addition to the present pressure loss due to flow through the duct. However, it is an option in further investigations analogue to the modeling of temperature loss.

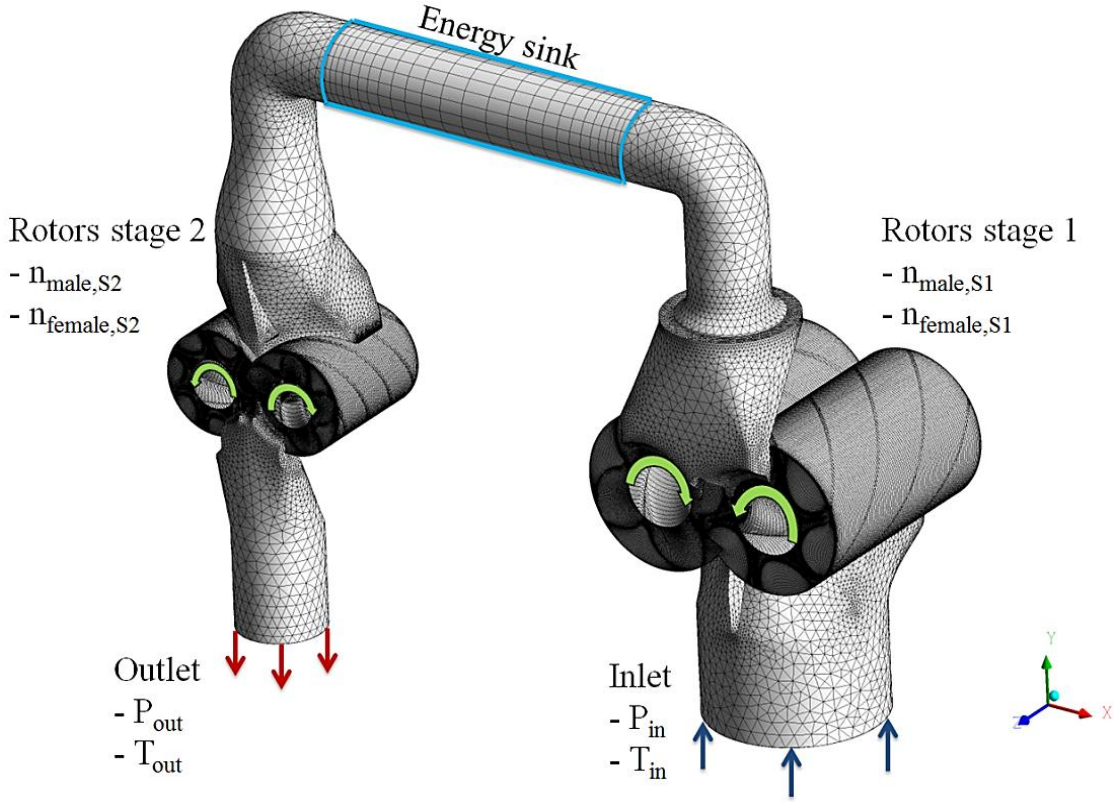

Figure 2: Numerical model of the screw compressor with boundary conditions and grid lines

The case is set up for three different operating points (OP), where the rotational speed of the stages is varied as well as inlet and outlet temperature (used only in case of backflow) according to the conditions indicated by experimental

data. In addition, one case with smaller housing clearances (uniformly decreased by approximately 20%) and smaller intermesh clearance (closest distance between the rotors decreased by approximately 50%) for each stage is simulated, while axial clearances remain unchanged.

Table 2 shows the four operating points taken into account:

Case	Main shaft speed [rev/min]	Inlet Pressure [bar(a)]	Outlet pressure [bar(a)]	Inlet temp. 1st stage [C]	Inlet temp. 2nd stage [C]	Outlet temp. 2nd stage [C]
OP1	1490	1.0	7.98	30.8	31.9	136.1
OP2	1790	1.0	7.98	28.6	34.1	143.0
OP3	2100	1.0	7.98	80.6	37.9	150.8
OP4 (Decreased radial clearances)	1790	1.0	7.89	28.6	34.1	143.0

Table 2: Boundary conditions for the performed simulations

The individual stages are driven by the main shaft over a friction gear. The female rotor speed of each stage is given by the lobe ratio between male and female rotor. The ratios are 2/3 for the first stage and 5/7 for the second stage.

All simulations are transient, where the angle increment was doubled by using every second of the generated rotor chamber grids. To model the accurate rotation speed of each rotor, the time step has to be doubled as well. The fluid is air as an ideal gas, with constant fluid properties except for the density. Turbulence is taken into account with the SST turbulence model. All walls are treated as adiabatic.

4. SIMULATION RESULTS

For both stages of the screw compressor, the compression inside the working chamber is visualized in Figure 3 by the instantaneous pressure distribution on the rotor walls. It is shown over one pitch angle of the corresponding stage. At the depicted rotor positions (0° to 60° for the first stage, 0° to 49° for the second stage), the pressure in the rotor chambers formed by male and female rotor lobes increases as the volume of the individual chambers is decreasing. Once the lobes reach the control edges, the connection of the chambers with the discharge port is established and compression process is finished.

Time averaged over one male rotor revolution, the discharge pressure of the first stage is 3.33 bar at 1790 rpm (average value on a plane, approx. 10 mm above the discharge port), where the suction pressure upstream of the second stage is 3.23 bar in average (average value on a plane, approx. 30 mm above the suction port). A time resolved depiction of discharge and suction pressure is given in Figure 4. This is in good comparison to the experiment, where for the same shaft speed, the discharge pressure of the first stage is about 3.5 bar. Inlet and outlet pressure (i. e. upstream of the first stage and downstream of the second stage), are at a fixed value as a boundary condition according to the experimental setup (see Table 2).

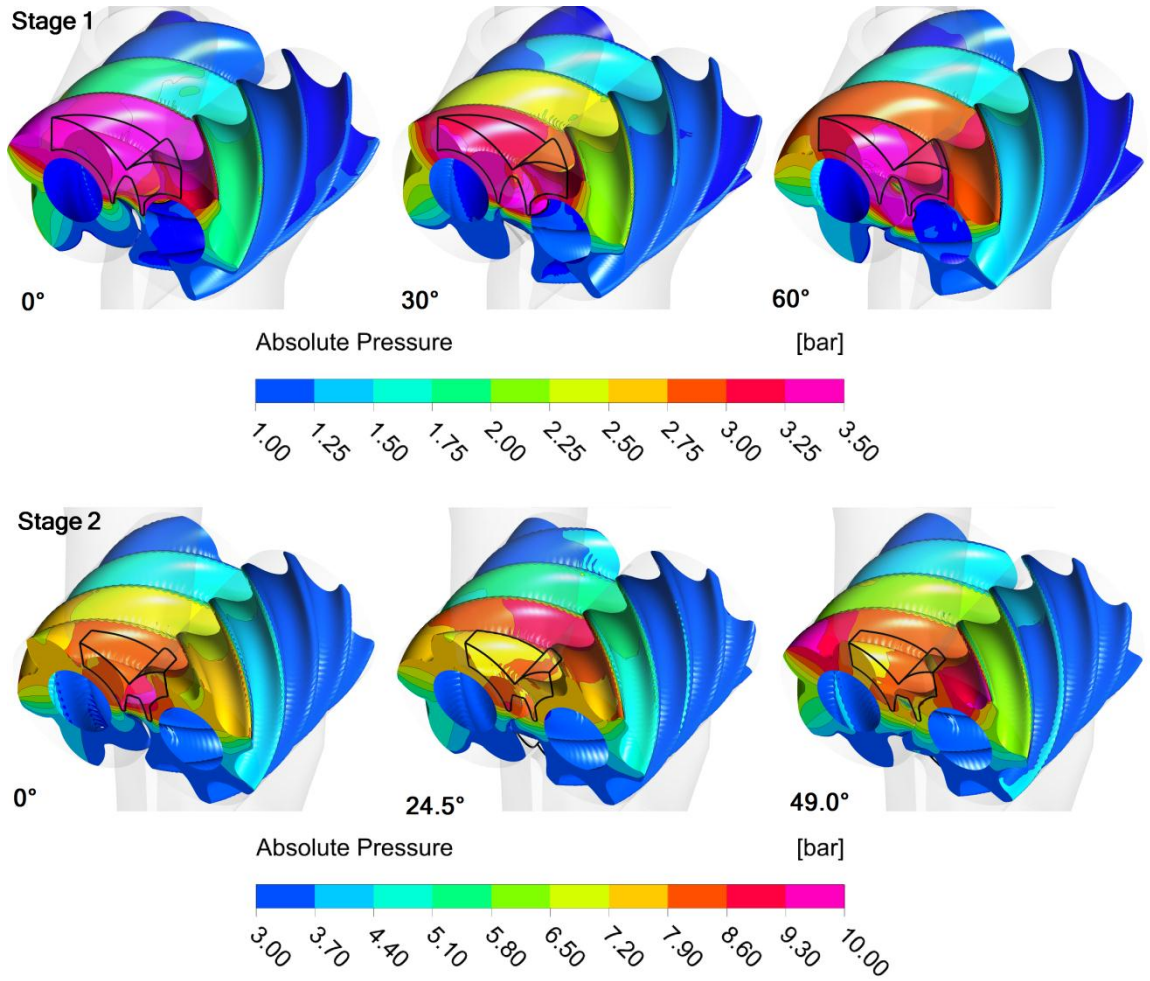

Figure 3: Instantaneous pressure distribution at 1790 rpm for first (top) and second stage (bottom) over one pitch angle

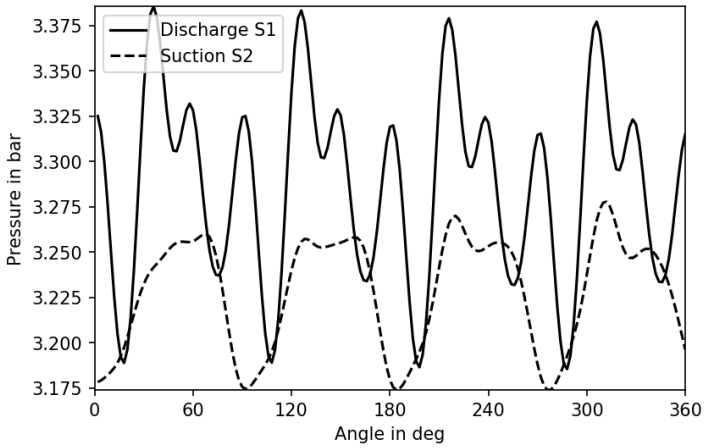

Figure 4: Discharge pressure of stage 1 (S1) and suction pressure of stage 2 (S2) over one male rotor revolution of the first stage at 1790 rpm

The velocity field as well as the temperature field on a plane within the duct is visualized in Figure 5. As specified by the applied energy sink within the duct, the temperature drops gradually in order to provide cooled air at the suction side of the second stage.

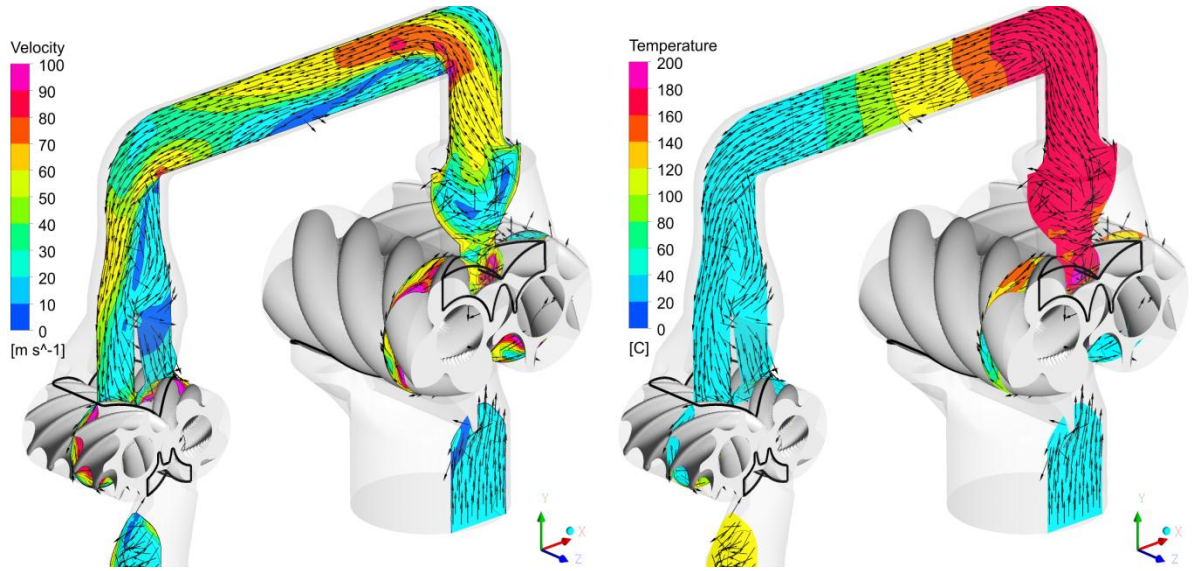

Figure 5: Instantaneous velocity and temperature field on a plane in the center of the duct between the two stages

The discharge temperatures at 1790 rpm of the first and second stage are quite constant with a maximum variation of about 8°C (first stage) and 0.5°C (second stage) respectively. The time averaged temperatures are approximately 163°C for the first stage and 128°C for the second stage. Measured in the experiment, the discharge temperature of the first stage is around 175°C and 158°C for the second stage.

The volumetric flow rates for all operating points at inlet and outlet of the compressor are shown in Figure 6. The given values correspond to the calculated mass flow rates divided by the reference density according to the inlet pressure and temperature. Due to numerical errors, the time averaged values of inlet and outlet flow rates are not exactly equal. However, the deviation is below 1% for all cases. The resulting volumetric flow rates are the mean values between inlet and outlet, each time averaged over 1 male rotor revolution of the first stage.

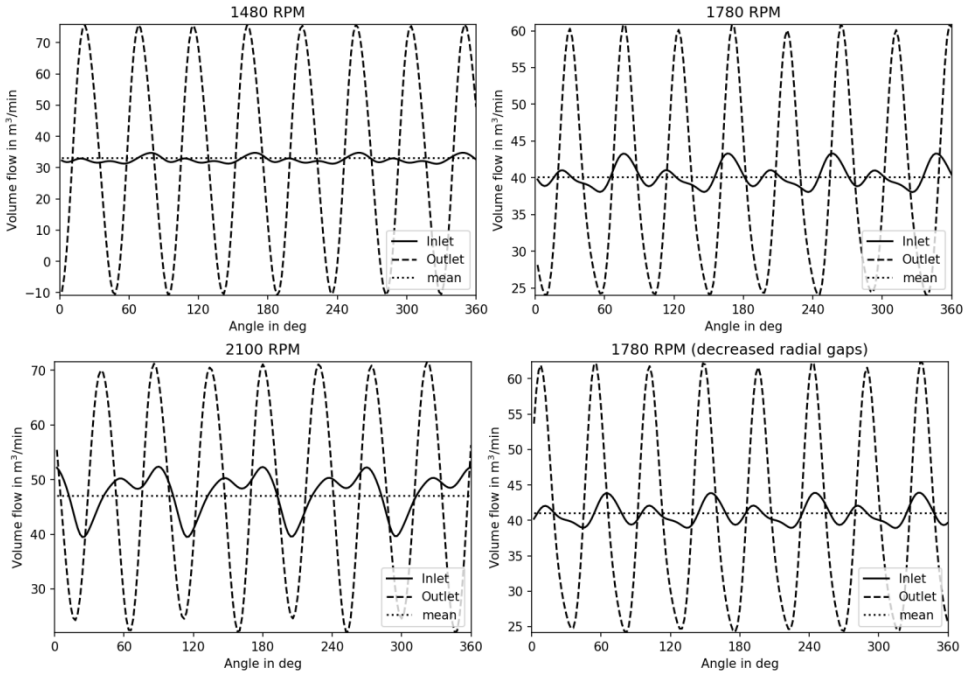

Figure 6: Volumetric flow rates at inlet and outlet of the compressor for the different operating points over one male rotor revolution of the first stage

An increase of the average flow rate with an increasing shaft speed is apparent (while inlet and outlet pressure are kept unchanged). For the lowest simulated shaft speed of 1480 rpm, also backflow at the outlet can be identified over a certain angle range. The flow rates are 32.6 m³/min at 1490 rpm, 40.3 m³/min at 1790 rpm and 47.5 m³/min at 2100 rpm shaft speed respectively. Qualitatively, it can be observed that the flow rate fluctuation at inlet and outlet is also more pronounced at higher shaft speeds.

Analogue to the flow rates, the indicated power is examined for all operating points. It is only calculated based on the torque which results from pressure forces acting on the rotors during the compression of the air inside the working chambers. Mechanical losses, like e. g. friction due to bearings, shaft sealing or lobe intermeshing are not included. Like the flow rates, power is increasing nearly linearly with rising shaft speed, what matches the expected behavior of the screw compressor. The calculated power for both stages combined is 188 kW at 1490 rpm, 230 kW at 1790 rpm and 276 kW for 2100 rpm respectively. For all shaft speeds, the first stage contributes about 55% of the total power. The time resolved power data are shown in Figure 7.

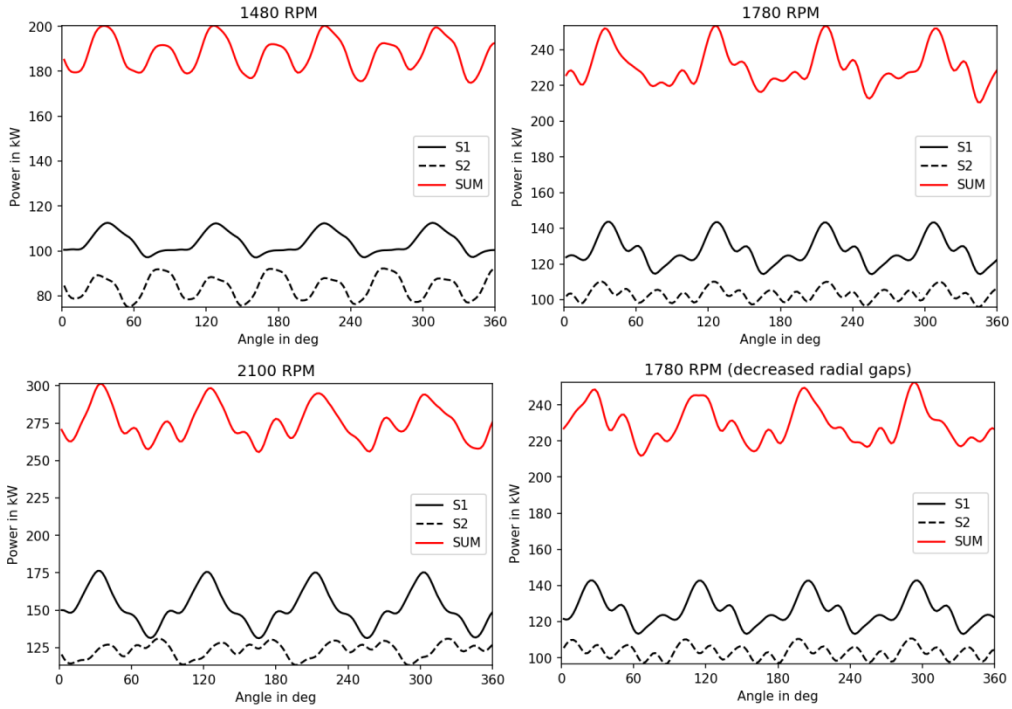

Figure 7: Power of the compressor for the different operating points over one male rotor revolution of the first stage

The simulation results are compared to measurements in Figure 8 and Table 3 of the real screw compressor in terms of measured volumetric flow, power and specific power.

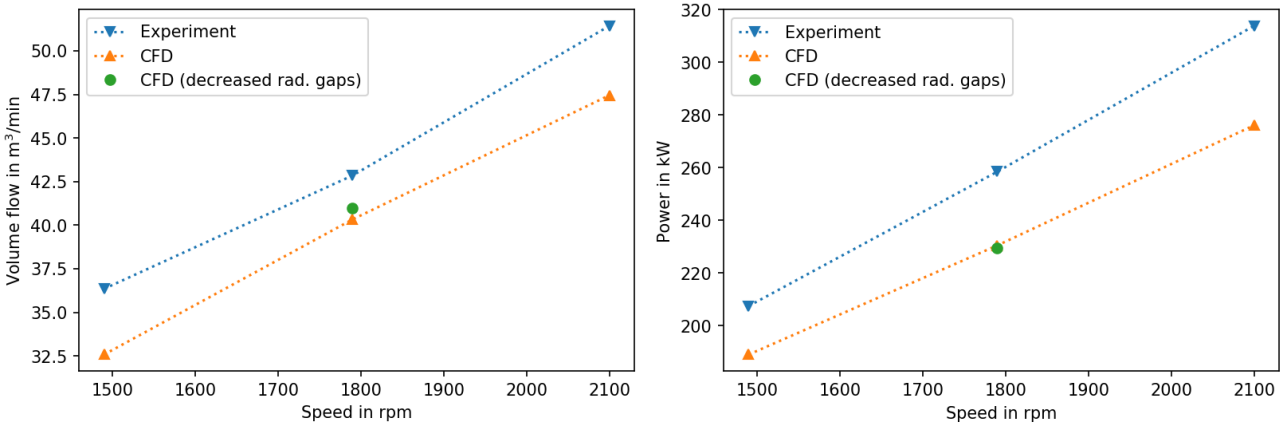

Figure 8: Comparison of experimental measurements and CFD results for all considered operating points

	Measurements			CFD Results			Relative Deviation		
	Flow Rate [m³/min]	Power [kW]	Specific Power [kW/(m³/min)]	Flow Rate [m³/min]	Power [kW]	Specific Power [kW/(m³/min)]	Flow Rate [%]	Power [%]	Specific Power [%]
OP1	36.35	207.4	5.705	32.58	188.0	5.770	-10.4%	-9.4%	1.1%
OP2	42.85	258.4	6.030	40.33	230.4	5.712	-5.9%	-10.8%	-5.3%
OP3	51.43	313.8	6.102	47.45	276.0	5.817	-7.7%	-12%	-4.7%
OP4	-	-	-	40.96	229.4	5.601	-4.4%	-11.2%	-7.1%

Table 3: Comparison of experimental measurements and CFD results for all considered operating points

It can be seen that volumetric flow rate as well as power are computed lower than measured for the real compressor. For the flow rates, CFD results are about 8% to 10% lower, whereas the power is about 9% to 12% lower. Given the lower flow rate, a lower power is evident. Hence, also the specific power is compared. Due to the lack of mechanical losses present in the CFD simulation, the specific power is expected to be lower than of the real compressor. This is the Case for OP2 to OP4, where the specific power is about 5% to 7% below the measured value. However, for OP1 the calculated value exceeds the experimental value by 1%. At this point it is not clear why this is the case and it needs further investigation. After all, it is noteworthy that the specific power for OP1 also deviates from OP2 and OP3 in the experiment.

A significant influence of the decreased clearances for 1790 rpm (i. e. the same as for OP2) cannot be observed, as flow rate and power remain approximately the same. Concerning the power, the averaged value is even slightly lower, whereas a higher value would be expected. One reason for the miniscule influence of the decreased clearances could be the utilized meshing strategy, where nodes are fixed on the stator curves and slide over the rotor walls. The 3D mesh including the twist angle is generated by 2D mesh slices where linear interpolation is present between the individual slices depending on the number of grid nodes in axial direction. Within the 3D mesh, this can lead to higher clearances than present in the 2D mesh slices. A different meshing strategy (e. g. fixing the grid nodes on the rotor curves instead of on the stator curves) could achieve better control over the gap sizes, however this approach was not realized because of the reasons stated in chapter 2 (i.e. the ability to combine both stages in one setup and using a small set of meshes to perform an arbitrary amount of time steps without interpolation).

In addition to direct comparison to experimental data of the real compressor, a simple estimation of the theoretical compressor power is done according to the Compressed Air and Gas Handbook (2016), assuming an isentropic compression:

$$\boldsymbol{P = \frac{Q_1 p_1}{64.85}\left[\left(\frac{p_2}{p_1}\right)^{(k-1)/k} - 1\right]} \tag{1}$$

In this estimation, $Q_1$is the volumetric flow rate at inlet conditions, $p_1$and p_2 the inlet and outlet pressure and k the isentropic exponent, which is about 1.4 for air. It should be noted that for this formula, pressure units are in psi and flow rates in cfm, where the theoretical power is in hp. For convenience, the results are presented in SI units hereinafter. Since this theoretical power assumes isentropic compression without any mechanical losses, the efficiency of the screw compressor can be taken into account. The total efficiency η_{tot} is given by Sullair for the individual operating points and includes all losses, i. e. thermodynamic and mechanical losses. Hence, the additional power due to the losses can be added to the theoretically determined power:

$$P_t = \frac{P}{\eta_{tot}} \tag{2}$$

The power estimation and comparison to both, measurements and CFD results is shown in Table 4. The theoretical assumption combined with the stated total efficiency by Sullair is very close to the measured power. Compared to the CFD results, it is also in good agreement. For OP1, the power is slightly overestimated by 0.5%, where it is about 6% to 8% lower for OP2 and OP4. This corresponds to the deviations regarding the specific power shown in Table 3. Analogue to the results for the specific power, it should also be noted here that a lower compressor power value would be expected for OP1 (i.e. it should be lower than the theoretical combined with the total efficiency). It remains uncertain if there are inaccuracies in the CFD calculation or the measurements as well as the determined total efficiency which is the basis of the theoretical power calculation.

		Measurements			Relative Deviation	CFD Results			Relative Deviation
	η_{tot} [%]	P [kW]	P_t [kW]	Power [kW]		P [kW]	P_t [kW]	Power [kW]	
OP1	82.01	171.1	208.6	207.4	-0.6%	153.3	187.0	188.0	0.5%
OP2	77.59	201.7	260.0	258.4	-0.6%	189.8	244.7	230.4	-6.2%
OP3	76.60	242.1	316.0	313.8	-0.7%	223.3	291.5	276.0	-5.6%
OP4	(77.59)	-	-	-	-	192.8	248.5	229.4	-8.3%

Table 4: Theoretical power estimation in comparison with experimental measurements and CFD results

5. CONCLUSION AND OUTLOOK

This paper shows a CFD approach to simulate the sample dry screw compressor provided by Sullair. This compressor consists of two compressor stages with an intermediate cooler. In the presented approach, both stages as well as the interstage cooling are modeled within one setup, allowing a direct coupling of the stages without the need to specify boundary conditions at the outlet of the first stage or at the inlet of the second stage respectively. The cooler is replaced with a simple duct, where the temperature drop (i. e. a specified suction temperature for the second stage is reached) is realized with an energy sink.

The simulations are performed for a total pressure ratio (both stages combined) of 7.98 for three different rotational speeds. In addition, for one shaft speed, radial clearances (i.e. housing and intermesh gaps) are reduced. The CFD results are compared with measurements of the real compressor. The values for the flow rate and compressor power are in good match with the experiment, so it is indicated that the overall working mechanism of the two stage compressor is appropriately captured. In general the simulations with reference clearances underestimate the flow rates by about 6% to 10%. The uncertainties regarding clearance sizes in the 3D mesh mentioned in chapter 4 are expected to contribute to these findings. Moreover it has to be noted that deformations due to pressure and temperature loads are not taken into account in the simulation. These deformations present in real compressors after heating up can also lead to a change in clearances sizes, affecting the flow rate. Being a highly complex machine, other influences like e. g. the flow conditions upstream, downstream and between the stages as well as the wall heat transfer, which are all neglected in the simulation approach, are expected to have a significant influence on the compressor performance.

However, the presented model serves for a solid basis to further investigations and allows including or enhancing neglected or simplified parts of the model (e. g. the intermediate cooler, the assumption of adiabatic walls or a better representation of the cooler regarding total pressure loss). Future work on the model will focus on a more detailed investigation of clearances and leakage flows and the associated meshing strategies. Also the heat transfer is of interest, thus rotor and stator solids as well as active cooling of stator components should be included to the existing model to validate and improve the simulation results. As a goal for the industry, a precise distinction and quantification of thermal and mechanical losses is desired in order to optimize their compressors.

NOMENCLATURE

P	Theoretical compressor power	[W]	k	Isentropic exponent	[-]
P_t	Theoretical compressor power including total compressor efficiency	[W]	Q_1	Volumetric flow rate at inlet conditions	[cfm]
η_{tot}	Total compressor efficiency	[%]	p_1, p_2	Suction and discharge pressure	[psi]

REFERENCES

Spille-Kohoff, A., Hesse J., El Shorbagy A. (2015). CFD simulation of a screw compressor including leakage flows and rotor heating. *9 th International conference on compressors and their systems (ICCS)*, London

Hesse J., Spille-Kohoff A., Hauser J., Schulze-Beckinghausen P. (2014). Structured meshes and reliable CFD simulations: TwinMesh for positive displacement machines. *9th International Conference on Screw Machines (ICSM),* Dortmund

Compressed Air & Gas Institute (2016). *Compressed Air and Gas Handbook (Seventh Edition)*, Cleveland